An RCS-Like Retinal Dystrophy Phenotype in *Mer* Knockout Mice

Jacque L. Duncan,[1] *Matthew M. LaVail,*[1,2] *Douglas Yasumura,*[1,2] *Michael T. Matthes,*[1] *Haidong Yang,*[1] *Nikolaus Trautmann,*[1] *Aimee V. Chappelow,*[1] *Wei Feng,*[3] *H. Shelton Earp,*[4,5,6] *Glenn K. Matsushima,*[7,8,9] *and Douglas Vollrath*[3]

Purpose. To determine whether mice that are homozygous for a targeted disruption of the *Mer* receptor tyrosine kinase gene (*mer*^{kd}) manifest a retinal dystrophy phenotype similar to RCS rats, which carry a mutation in the orthologous gene *Mertk*.

Methods. Eyes of *mer*^{kd} and C57BL/6 wild-type (WT) mice were examined by light and electron microscopy, whole-eye rhodopsin measurement, and Ganzfeld electroretinography (ERG).

Results. The *mer*^{kd} mice showed rapid, progressive degeneration of the photoreceptors (PRs). Features of the phenotype common to *mer*^{kd} mice and RCS rats included the absence or near absence of phagosomes in the retinal pigment epithelium (RPE) at the peak of outer segment (OS) disc shedding, accumulation of debris and whorls of membranes at the RPE-OS interface, transient supernormal rhodopsin content and OS lengths, the presence of OS vacuoles beginning at early ages, and a relatively slow removal of pyknotic PR nuclei. Most PRs were missing, and OS debris was removed by approximately postnatal day (P)45. Scotopic ERG responses were lower than age-matched WT responses and declined with PR loss. Photopic responses were preserved better than scotopic responses, corresponding with preferential cone preservation as judged histologically. ERG amplitudes were usually unmeasurable beyond P40, although a small-amplitude scotopic threshold response (STR) could still be elicited at P253 in some mice when only scattered PR nuclei remained.

Conclusions. Ablation of *Mer* function in *mer*^{kd} mice results in a retinal phenotype almost identical with that of RCS rats. The similarity in phenotypes between the two rodent models suggests that an RPE phagocytic defect is a feature of all types of retinal degeneration caused by loss of function of Mer tyrosine kinase, perhaps including mutations in human *MERTK*. (*Invest Ophthalmol Vis Sci.* 2003;44:826–838) DOI:10.1167/iovs.02-0438

Inherited and age-related retinal degenerations are a group of diseases that share progressive dysfunction and death of photoreceptors (PRs). Retinitis pigmentosa affects approximately 1 in 3500 to 4000 people worldwide. A more common condition, age-related macular degeneration (AMD), affects an estimated 6 million people in the United States alone, and this number is expected to increase in the future, because the elderly population will double over the next 30 years.[1]

AMD shares other features with some inherited retinal degenerations. For example, abnormalities of the retinal pigment epithelial (RPE) cells are a feature of AMD,[2–4] and specific RPE defects are seen also in several inherited degenerations such as Best disease,[5,6] Stargardt disease,[7] Sorsby fundus dystrophy,[8,9] childhood-onset severe retinal dystrophy,[10] and Leber congenital amaurosis due to mutations of RPE65.[11–14] RCS rats have been studied extensively as a model of retinal degeneration[15,16] and PR-RPE cell interactions.[16,17] The primary defect responsible for the RCS phenotype is failure of the RPE to phagocytize shed rod outer segments (OS).[18,19] The unphagocytized OS membranes form membranous whorls at the RPE surface, and the rod OS grow abnormally long.[20,21] Eventually, the OS layer degenerates into a debris zone with subsequent PR cell death.[20]

Recently, positional cloning was used to identify a null mutation in the receptor tyrosine kinase *Mertk* gene in RCS rats.[22] *Mer* is the official designation for the murine gene that is orthologous to rat and human *Mertk*. Mer is a member of the Axl/Mer/Tyro3 receptor tyrosine kinase subfamily. The growth-arrest–specific protein 6 (Gas6) is a ligand for all three members of this subfamily.[23–25] Gas6 binds to the receptors through its carboxyl-terminal half,[26] whereas an N-terminal domain of Gas6 that is rich in γ-carboxylated glutamic acid residues mediates binding to phosphatidylserine.[27] Phosphatidylserine molecules normally are localized to the inner membrane leaflet, but are exposed on the exterior of apoptotic cell membranes.[28] It has been suggested that Gas6 may mediate RPE phagocytosis of OS by binding to and serving as a bridge between older OS membranes and Mer.[22] In support of this model, purified Gas6 has been shown to stimulate phagocytosis of OS by cultured RPE cells.[29] Moreover, Mer localizes to the sites of OS uptake and appears to trigger the ingestion step of RPE phagocytosis in cell culture.[30] Several other RPE cell surface proteins have been implicated in the binding or internalization of OS,[31,32] such as $\alpha v\beta 5$ integrin,[33] CD36,[34] and the mannose receptor,[35,36] but there is no current evidence that these molecules are causally related to the degeneration of PRs.

A viral vector was used recently to transfer wild-type (WT) *Mertk* to the RPE of RCS rats. This resulted in reversal of the RPE phagocytosis defect and PR rescue,[37] which conclusively demonstrated that mutation in *Mertk* is the cause of retinal degeneration in RCS rats. Mutations in human *MERTK* have

From the [1]Department of Ophthalmology, Beckman Vision Center, and the [2]Department of Anatomy, University of California, San Francisco, California; the [3]Department of Genetics, Stanford University School of Medicine, Stanford, California; the Departments of [4]Pharmacology, [6]Medicine, and [7]Microbiology and Immunology, the [5]Lineberger Comprehensive Cancer Center, the [8]University of North Carolina Neuroscience Center and the [9]Program for Molecular Biology and Biotechnology, University of North Carolina, Chapel Hill, North Carolina.

Supported by a Career Development Award from Research to Prevent Blindness (JLD); National Eye Institute Grants EY01919, EY02162 (MML), and EY00415 (JLD); the Ruth and Milton Steinbach Fund and the Karl Kirchgessner Foundation (DV); the Foundation Fighting Blindness, Inc.; the Macular Vision Research Foundation (MML); a postdoctoral fellowship from the Fight for Sight Division of Prevent Blindness America (WF); and That Man May See, Inc. MML is a Research to Prevent Blindness Senior Scientist Investigator.

Submitted for publication May 2, 2002; revised August 7, 2002; accepted August 19, 2002.

Commercial relationships policy: N.

The publication costs of this article were defrayed in part by page charge payment. This article must therefore be marked "*advertisement*" in accordance with 18 U.S.C. §1734 solely to indicate this fact.

Corresponding author: Matthew M. LaVail, Beckman Vision Center, UCSF School of Medicine, 10 Koret Way, Room K-120, San Francisco, CA 94143-0730; mmlv@itsa.ucsf.edu.

been identified in patients with retinitis pigmentosa.[38] *Mer* defects in other species could help to elucidate the role of *Mer* in RPE cell phagocytosis and retinal degeneration. A mouse strain with targeted disruptions of the genes encoding Tyro3, Axl, and Mer has been produced.[39] These mice were described as blind due to postnatal degeneration of rods and cones, but no retinal histologic or electrophysiological results were presented. A mouse strain carrying only the targeted disruption of *Mer* (*mer^{kd}*) has also been produced that exhibits hypersensitivity to endotoxins[40] and a generalized defect in phagocytosis of apoptotic thymocytes by macrophages.[41] The retinal phenotype of these mice has not been previously investigated. Herein we present structural and functional characteristics of the retinal phenotype of *mer^{kd}* mice. Because the gene mutated in these mice is orthologous to the mutant gene responsible for retinal dystrophy in RCS rats, we examined *mer^{kd}* mice for all the key retinal phenotypic characteristics of RCS rats.

Methods

Mice

All studies were conducted in accordance with the ARVO Statement for the Use of Animals in Ophthalmic and Vision Research. *Mer^{kd}* mice were bred from the same stock as previously described[41] and compared with age-matched C57BL/6 WT mice raised in the same facility. Mice were maintained in a 12-hour light–dark cycle at an in-cage illuminance of less than 10 ft-c.

Immunoblot Analysis

Retina/sclera and kidney were dissected from 4-month-old *mer^{kd}* and C57BL/6 mice and homogenized in 1% NP-40 lysis buffer (50 mM Tris-HCl, 150 mM NaCl, 2 mM EDTA, 1% NP-40 [pH 8.0]) containing a protease inhibitor cocktail (Roche Molecular Biochemicals, Mannheim, Germany). Glycoproteins were enriched by wheat germ agglutinin (WGA)-Sepharose beads (Sigma, St. Louis, MO) as described,[30] separated by 6% SDS-PAGE and transferred to a nitrocellulose membrane (Fisher Scientific, Pittsburgh, PA). Mer tyrosine kinase protein was detected by a polyclonal antibody directed against the C-terminal part of rat Mertk[30] or by a polyclonal antibody directed against the ectodomain of murine Mer (R&D Systems, Minneapolis, MN), followed by a horseradish peroxidase–conjugated secondary antibody and chemiluminescence (Super Signal West Pico Chemiluminescent Substrate system; Pierce, Rockford, IL).

Histologic Analysis

At different ages (Table 1) mice were killed with carbon dioxide inhalation and immediately perfused intracardially with a mixture of aldehydes (2% paraformaldehyde and 2.5% glutaraldehyde). Eyes were removed, bisected along the vertical meridian, postfixed in osmium tetroxide, and embedded in an Epon-Araldite mixture. Sections of the entire retina were cut 1-μm thick and stained with toluidine blue, as described elsewhere.[21] The thickness of the outer nuclear layer (ONL) was taken as a measure of PR number,[42] and the mean ONL and rod OS thickness were obtained from 54 measurements around the retina, as described elsewhere.[43] Tissue sections were chosen where the rod OS and Müller cell processes crossing the inner plexiform layer were continuous in the plane of the section, or nearly so, to assure that the sections were not oblique. Electron microscopy was used for ultrastructural evaluation of the retinas at selected ages by previously described methods.[44]

To study rod OS disc shedding and phagocytosis by the RPE, we perfusion fixed four *mer^{kd}* and four WT mice (two each at postnatal day [P]15 and P20 for each genotype) between 1 and 1.5 hours after the onset of light in the morning. We quantified the number of phagosomes in the RPE cell processes and cell bodies by light microscopy with ×100 oil-immersion optics at ×1000 magnification (Axiophot; Zeiss, Thornwood, NY), according to previously described criteria.[45] These required that the phagosome, either in the RPE cell processes or in the RPE cell body, be greater in any dimension than 0.75 μm (half the rod OS diameter) and stain more densely than the OS.[45] Thus, smaller intensely staining structures (e.g., residual bodies, lipid droplets, and mitochondria) were not counted. The rationale for including in the phagosome counts the densely staining shed packets of rod OS discs located in the RPE cell processes is discussed elsewhere.[45] The entire retinal length was examined (i.e., >4 mm) in a single, midsagittal section from each animal.

Table 1. Number and Ages of Mice Studied

	Histology		Rhodopsin		ERG	
Age (P)*	*mer^{kd}*	WT	*mer^{kd}*	WT	*mer^{kd}*	WT
2	3	2				
4	3	2				
6	4					
8	6	2				
10	5 (2)	5 (2)				
12	4 (3)	4 (3)				
15	4 (4)	4 (3)				
20	11 (7)	6 (5)			3	4
25	3 (3)	4 (3)	10	10	3	2
30	2 (2)	2 (2)			2	5
32	2					
33	2 (2)	3 (3)			6	3
36	10 (7)	9 (3)			9	4
40	8 (7)	5 (3)	8	8	7	4
45	5 (3)	5 (0)				
50	4 (2)	5 (3)			4	2
58	4 (3)		4	4	4	1
65	2 (2)				2	
72	1				1	
77	4 (2)	4			2	
80						3
85	1 (1)	4 (3)				
100						2
118		4				
150	1	2				
180		4				3
186	2 (2)				2	
197	1				1	
240	3				2	1
255	4	4			4	1
365	2	4				
400						2

P, postnatal day; numbers in parentheses indicate numbers of eyes in which ONL thickness was quantified.

* Age of each animal was ±1 day at P20 and older.

Rhodopsin Measurements

Mice were dark adapted overnight, and all procedures were performed in dim red light. Both eyes from each mouse assayed (Table 1) were pooled after lens removal and homogenized in 0.85 mL 20 mM (3-*N*-morpholino) propane sulfonic acid (MOPS) containing 1.5% lauryl maltoside[46,47] and 0.2 M hydroxylamine hydrochloride. The homogenate was extracted on ice for 3 hours and centrifuged for 15 minutes at 135,000*g* at maximum rotation (r_{max}) in a centrifuge (TL100; Beckman Instruments, Carlsbad, CA). The change in absorbance at 498 nm was measured with a spectrophotometer (Genesys 5; Spectronics, Westbury, NY) after bleaching for 60 seconds at a distance of 10 cm with a 60-W bulb and used to calculate the whole-eye rhodopsin content (absorbance coefficient of rhodopsin at 498 nm = 42,000 M/cm).[48]

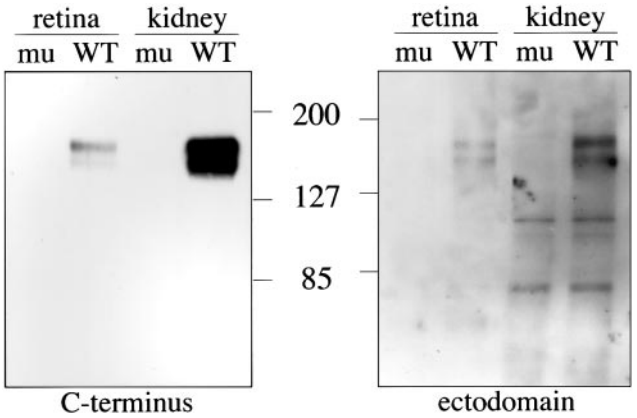

FIGURE 1. Absence of Mer protein in tissues from *mer*^{kd} mice. Protein lysates from the retina/sclera and kidney of *mer*^{kd} mutant (mu) and B6 (WT) mice were tested for Mer protein by immunoblot analysis, with polyclonal antisera directed against the C-terminal 100 amino acids of the rat Mer tyrosine kinase (*left*) or against the ectodomain of mouse Mer (*right*).[30] A doublet of Mer bands (~150 and ~170 kDa) is detected in WT tissues, but is absent from *mer*^{kd} tissues. The two bands are differentially glycosylated forms of the receptor.[30]

Electroretinographic Analysis

Electroretinograms were recorded as described previously[37] on *mer*^{kd} mice and WT mice at several ages (Table 1). Photopic a-waves were not quantified, because WT mice have negligible photopic a-waves.[49] Threshold criterion amplitudes were 20 μV for scotopic b-waves and 10 μV for photopic b-waves. Thresholds and implicit times for a-waves were not measured because of interference from the cornea-negative scotopic threshold response (STR) observed between b-wave threshold and the normal a-wave threshold.

N-methyl-DL-aspartic acid (NMA; Sigma) suppresses synaptic transmission by acting primarily on third-order neurons[50–52] and has been used to distinguish between the a-wave and the STR, both of which are cornea-negative ERG waveforms, in cats[50,51] and RCS rats.[52] To confirm that the negative ERG waveform observed at dim stimulus intensities in WT and young *mer*^{kd} mice was the STR, NMA was injected intravitreally before recording the ERG, as previously described in RCS rats.[52] NMA was dissolved in 0.9% saline and passed through a 0.2-μm filter. The adult mouse vitreous volume was calculated from the schematic rat eye,[53] assuming the mouse vitreous volume to be one fourth as large as the vitreous volume of an adult rat. A 0.5-μL intravitreous injection of NMA was given with a 30-gauge beveled needle attached to a 10-μL syringe (Hamilton, Reno, NV) through the limbus under dim red illumination into one eye of older wild-type (WT) and age-matched *mer*^{kd} mice, for an estimated final vitreous concentration of 5 mM NMA.[52] The contralateral eye received a 0.5-μL intravitreous injection of normal saline to serve as the control. After the NMA was injected and the mice were prepared for ERG under dim red light, the mice were kept in darkness for an additional 45 minutes before the ERGs were recorded.

Statistical Analysis

The unpaired two-tailed Student's *t*-test with the Welch correction for unequal variance was performed on computer (Prism, ver. 3.00 for Windows; GraphPad Software, San Diego, CA) to compare data from *mer*^{kd} mice and age-related WT mice. The Pearson correlation coefficient was used to calculate the coefficient of determination (r^2), to correlate rates of structural and functional retinal degeneration.

RESULTS

Assessment of Mer Protein

The *mer*^{kd} allele was generated by targeted deletion of an exon encoding an essential portion of the *Mer* tyrosine kinase domain, presumably leading to premature termination of translation and ablation of the receptor's kinase activity. It is not certain that this mutation results in a complete loss of function. Indeed, the mutation was not intended to be a null allele.[40] The abundance of the mutant mRNA is similar to that of the WT mRNA,[39] which indicates that the *mer*^{kd} allele has the potential to produce a truncated protein. Mertk protein cannot be detected in RCS rat tissues,[30] indicating that the retinal dystrophy gene *rdy* is a null allele. We tested protein samples from the retinas and kidneys of WT and *mer*^{kd} mice for the presence or absence of Mer protein, using polyclonal antisera directed against either the cytoplasmic tail or the ectodomain of the receptor. Both antibodies detected Mer proteins of the expected sizes in tissues from WT animals (Fig. 1). By contrast, Mer protein was not detected in tissues from *mer*^{kd} mice, and there was no evidence of a truncated protein. These data indicate that *mer*^{kd} is a null allele. Comparison of the retinal phenotype of *mer*^{kd} mice and RCS rats is therefore warranted.

General Histologic Characteristics of PR Degeneration

As in RCS rats,[21] PR degeneration in *mer*^{kd} mice led to progressive thinning of the ONL over time (Fig. 2). The ONL thickness in *mer*^{kd} mice was indistinguishable from WT at P20 and younger but was significantly less than in age-matched WT

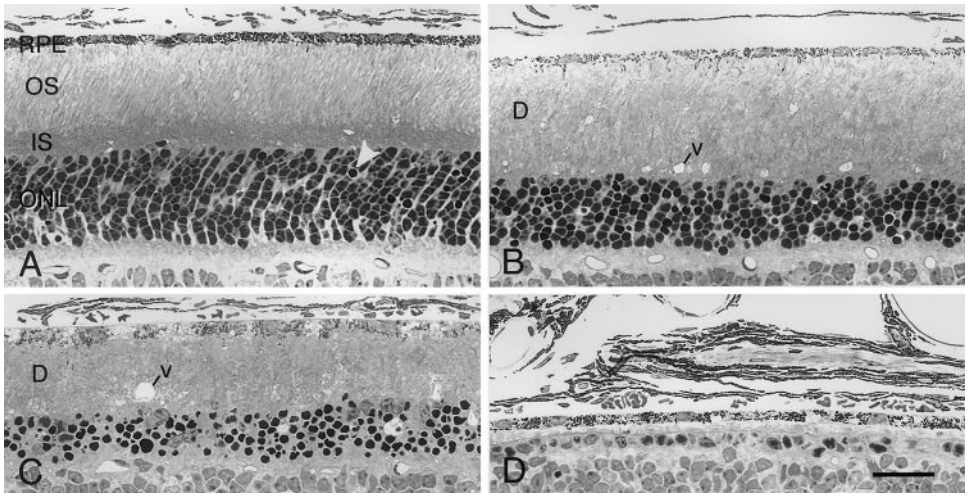

FIGURE 2. Light micrographs from the posterior retinas of *mer*^{kd} mice at P21 (**A**), P30 (**B**), P39 (**C**), and P45 (**D**). (**A–C**) Progressive degeneration of the ONL. The PR inner segments (IS) are lost with increasing age, and the outer segments (OS) become a membranous debris zone (D). A few pyknotic nuclei are seen at P21 (**A**, *arrowhead*), but many pyknotic nuclei are present at P30 (**B**) and P39 (**C**). (**D**) Advanced PR cell loss and loss of the debris zone. v, vacuole. Bar, 25 μm.

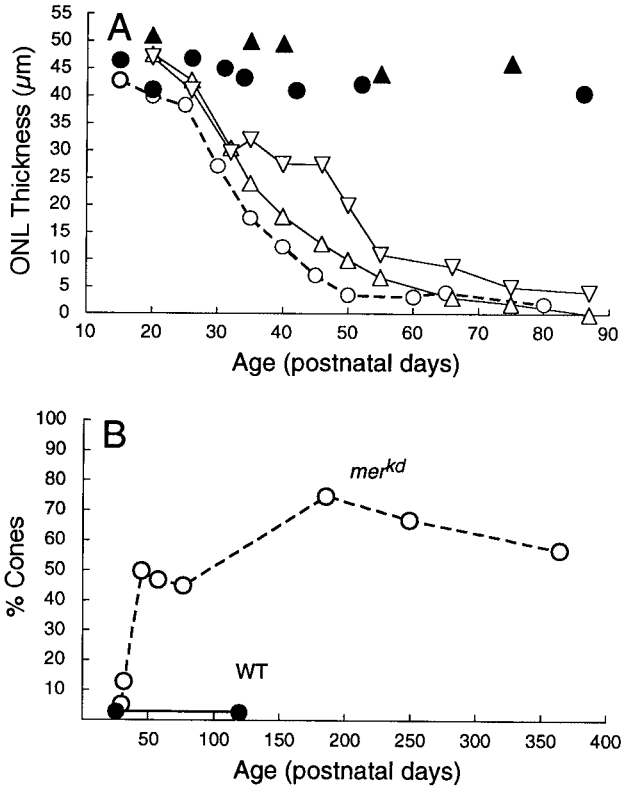

FIGURE 3. (**A**) ONL thickness at different ages in the posterior retina of black-eyed *mer*^{kd} (○) and WT (●) mice; pink-eyed RCS (△), black-eyed RCS-p/+ (▽) and normal Fischer albino (▲) rats. For mice, each point represents the mean of 12 measurements; 6 measurements were made on each side of the optic nerve head in two sections from at least three different eyes. Measurements were made at approximately 15-μm intervals, beginning approximately 300 μm from the optic nerve head. Rate data reprinted with permission from LaVail MM, Battelle BA. Influence of eye pigmentation and light deprivation on inherited retinal dystrophy in the rat. *Exp Eye Res.* 1975;21:167–192. (**B**) Percentage of surviving PR nuclei that were cones in the posterior retinas of *mer*^{kd} (○) or WT (●). Each value represents the mean percentage based on counts of surviving (nonpyknotic) PR nuclei in 10 195-μm lengths of retina after skipping 100 μm on each side of the optic nerve head for mice less than P77. In older mice in which far fewer surviving PRs were found, all remaining nonpyknotic PR nuclei in the retinal sections were tabulated. Each time point represents the mean of two to three mice. Rods are preferentially lost during PR degeneration in *mer*^{kd} mice. WT cone data adapted with permission from Carter-Dawson LD, LaVail MM, Sidman RL. Differential effect of the *rd* mutation on rods and cones in the mouse retina. *Invest Ophthalmol Vis Sci.* 1978;17:489–498.

mice at P25 ($P < 0.01$) and thereafter (Fig. 3A). The ONL thickness was less than one complete row of cell nuclei by P45 in most *mer*^{kd} mice (Fig. 2D). Beyond P45, some variability in the degree of PR cell loss was observed, with a few *mer*^{kd} mice retaining a single row of ONL cell nuclei in some parts of the retina up to approximately P60, whereas others had less than one row throughout the retina (Fig. 3A). At ages older than P90 (Table 1), there were progressively fewer PR surviving nuclei, but at least a few surviving nuclei were found in each section, even at the oldest ages. Although *mer*^{kd} mice are pigmented animals, the rate of retinal degeneration in the *mer*^{kd} mouse strain was similar to, if not slightly more rapid than, the rate of degeneration in pink-eyed RCS rats (Fig. 3A).

Because the ONL cells degenerated in *mer*^{kd} mice, the percentage of surviving cone PRs increased as the rod PRs preferentially degenerated. By 2 months of age approximately 50% of the surviving PRs were cones (Fig. 3B), and the percentage increased to a maximum of 75% at 6 months of age (Fig. 3B). RCS rats have been reported to show a similar pattern of cone preservation relative to rods during retinal degeneration.[54]

Pyknotic nuclei were observed in greater numbers in the ONL of *mer*^{kd} mice than in WT mice as early as P20. As PRs degenerated, many pyknotic nuclei were seen in the thinning ONL between P25 and P59 (Figs. 2B–D, 4A). The percentage of nuclei in the ONL that were pyknotic in *mer*^{kd} mice reached as high as 71% at P40 (Fig. 4A). A similarly high percentage of pyknotic cells in the ONL have been reported in RCS rats,[21] but this phenomenon is not typically seen in other animal models of retinal degeneration. When we examined a line of mutant rhodopsin transgenic rats that has a rate of PR degeneration comparable to that of *mer*^{kd} mice,[55] we found less than 3% of the ONL nuclei to be pyknotic at any given age (Fig. 4A). At P39 to P40, some of the pyknotic nuclei in the ONL of *mer*^{kd} mice coalesced and formed large masses of residual heterochromatin (Fig. 4B), a feature also observed in RCS rats.[21]

Some hemispheric differences and gradients of PR degeneration in RCS rats were either less pronounced or not observed in *mer*^{kd} mice. For example, in pigmented RCS rats a significant difference in the rate of degeneration has been found between the superior and inferior hemispheres, with ONL cell loss in the inferior hemisphere occurring more rapidly than in the superior hemisphere.[21] In *mer*^{kd} mice studied between P30 and P40, a similar pattern was observed, with a trend toward more rapid degeneration in the inferior retina. However, the difference was only approximately 5 μm, or one cell nucleus, and was statistically significant only at P36 and P40. RCS rats also show a distinct central–peripheral gradient of cell loss. Degeneration in the peripheral retina is slowed by approximately 10 days compared with the degeneration in the posterior pole.[21] In contrast, the *mer*^{kd} mice showed little, if any, consistent difference in the rate of degeneration in the posterior and peripheral retina.

Evidence of an RPE Phagocytic Defect

Before PR cell death during retinal degeneration, RCS rats show a failure to phagocytize rod OS.[18,19,44] There are several presumptive consequences of this defective phagocytosis, including the formation of membranous whorls adjacent to the RPE surface, longer than normal OS, and increased rhodopsin content in the eye. Each of these features of RCS rats was seen in *mer*^{kd} mice. Early in the degeneration, some membranous whorls were present at the RPE surface (Fig. 5B). Electron microscopic examination showed the whorls consisted of disorganized OS membranes and RPE cell processes (Fig. 6A). At P21, a few OS were present that reached the RPE surface, or nearly so (Fig. 6A), and although some OS were relatively intact (Fig. 6A), OS structure was not as orderly as in WT mice. At later ages, the OS degenerated further, and a debris zone nearly replaced the inner segment and OS layer (Figs. 2B, 2C). However, electron microscopic examination showed that some fragments of OS still were present, and some still reached the RPE cell surface at P37 (Fig. 6B). By P45, the whorls, abnormal OS, and membranous debris had disappeared in most *mer*^{kd} mice (Fig. 2D), although small pockets of debris membranes were seen in a few animals after this age.

By P20, the rod OS were significantly longer in *mer*^{kd} mice than in WT mice (Fig. 5). This abnormal increase in OS length (Fig. 7A) was accompanied by an increase in whole-eye rhodopsin concentration in *mer*^{kd} mice (Fig. 7B) at young ages, a feature also of RCS rats.[20,21] At P25, whole-eye rhodopsin concentration was 67% greater in *mer*^{kd} than in WT mice ($P < 0.005$), whereas OS length was increased by 33% ($P < 0.02$). At

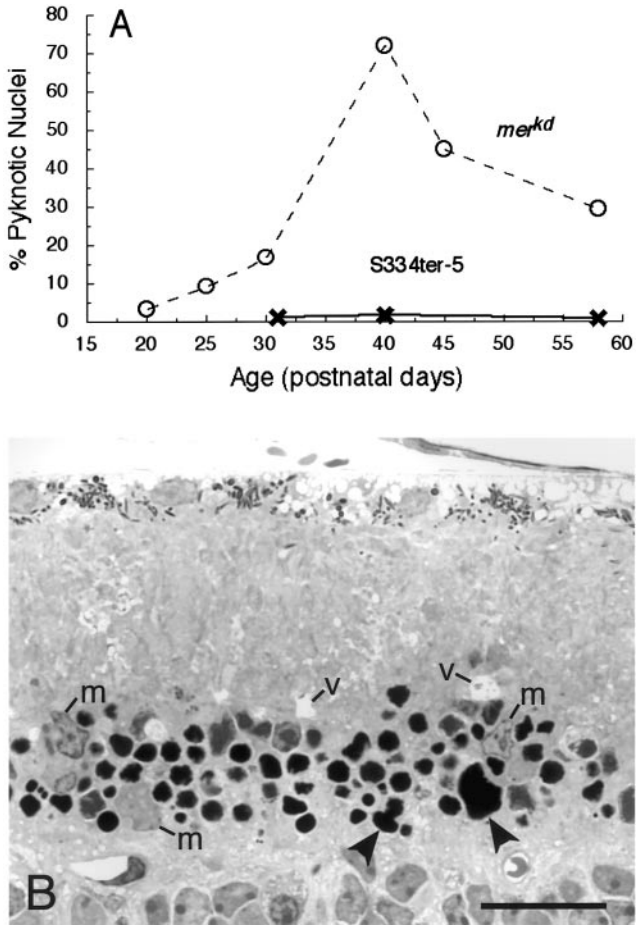

FIGURE 4. Many pyknotic PR cell nuclei are present in the ONL throughout the degeneration in *mer^kd mice.* (**A**) Percentage of surviving PR cell nuclei in the ONL that are pyknotic in *mer^kd* mice (○) and in S334ter-5 mutant rhodopsin transgenic rats (**X**). The transgenic rats share a similar rate of degeneration with the *mer^kd* mice,[55] but a much larger percentage of the surviving ONL nuclei are pyknotic in the *mer^kd* mice. In mice younger than P40 approximately 200 cells were measured in each of three areas in two hemispheres, whereas in older mice all cells were measured, and the percentage of cells that were pyknotic was calculated. Each time point represents the mean percentage of two animals. (**B**) Some pyknotic nuclei coalesce and form large masses of residual heterochromatin (*arrows*; age P39). Some large vacuoles (v) and invading macrophages (m) are present in the inner segment zone of debris. Bar, 20 μm.

P40, the OS length in *mer^kd* mice was significantly shorter than in WT ($P < 0.005$), whereas rhodopsin levels were approximately equal in the two genotypes ($P < 0.5$) (Fig. 7B). By P60, almost all OS membranes and rhodopsin were undetectable (Fig. 7).

To look for direct evidence of phagocytosis, we studied mice soon after the onset of light, at the peak of circadian rod OS disc shedding.[45] We examined retinas at two ages (P15 and P20), when rod OS were present but little or no accumulation of debris membranes or PR cell death were yet obvious. In WT mouse retinas, numerous phagosomes were observed in the apical RPE cell processes and RPE cell bodies (Figs. 5A, 8). The number of phagosomes at the peak of disc shedding in the WT mice was comparable to that found in the same strain of WT mice by others.[56,57] In contrast, few if any phagosomes were identified in *mer^kd* mice during the peak period of rod OS disc shedding (Figs. 5B, 8). In counts of phagosomes during the expected burst of disc shedding (Fig. 8), almost 74% of the 570 total phagosomes tabulated for the WT retinas were found in the RPE cell processes, as often is seen in albino rats during this period of disc shedding.[45] In the *mer^kd* retinas, however, only 3 of the 35 total profiles tabulated as phagosomes were located in the RPE cell processes. In the RPE cell bodies of *mer^kd* mice, no typical phagosomes were seen by light microscopy, but any structure that was definitely not a melanosome was tabulated for comparison with the WT. In the many mice of various ages whose eyes were harvested at different times of the day (Table 1), we frequently saw a few phagosomes in the retinal sections of WT mice, as expected during the nonpeak period of disc shedding.[45] In the *mer^kd* mice, however, we never observed any such phagosomes. Electron microscopic examination also did not reveal any typical phagosomes in *mer^kd* mice, although a few profiles were seen in which some apparent disc membranes were surrounded by RPE cytoplasm. None of these profiles showed highly condensed OS membranes characteristic of typical phagosomes,[45,58] and it is therefore possible that the packets of disks may not have been internalized by the RPE cells.

OS Vacuoles

At many ages in *mer^kd* mice, vacuoles were observed in the OS zone in well-fixed tissue (Figs. 2B, 2C). Similar vacuoles have been seen in RCS rats at all ages when OS or debris membranes were present (LaVail MM, unpublished observations, 2000), but have not been described previously. Retinas of *mer^kd* and WT mice were examined from P2 to P60, and the size and number of vacuoles were quantified. No vacuoles were identified in either WT or *mer^kd* retinas younger than P8. However, as early as discrete OS could be seen (beginning at P8 and P10), many vacuoles were found in *mer^kd* retinas (Fig. 9A), and they were evident at each age examined (Figs. 2B, 2C, 9B) up to P60. Most of the vacuoles in *mer^kd* mice were greater than 5 μm in diameter (Fig. 9B), and some were extremely large, reaching up to 35 μm in length. These structures were found in tissues fixed either by vascular perfusion or immersion, and very few vacuoles of this type were found in WT retinas at comparable ages. In some cases, none were seen in WT retinas (Fig. 9B). Most of the vacuoles in *mer^kd* retinas appeared to contain delicate fragments when viewed by light microscopy (Figs. 2B, 2C, 4B, 9A). When examined by electron micros-

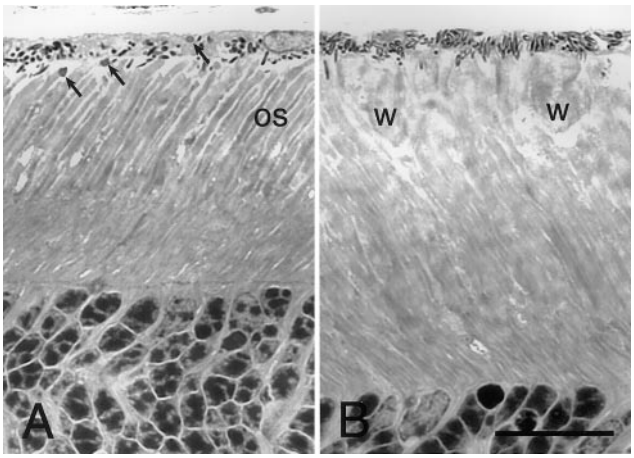

FIGURE 5. Light micrographs from *mer^kd* and WT mice at P20. Eyes were harvested 1 hour after light onset. (**A**) The WT mouse retina show an organized OS layer and numerous phagosomes (*arrows*). (**B**) The *mer^kd* mouse retina shows some membranous whorls (w) at the RPE surface, and the OS layer is much longer than in the age-matched WT. In addition, no phagosomes are observed, and some vacuoles are present in the inner segment and OS zone. Bar, 20 μm.

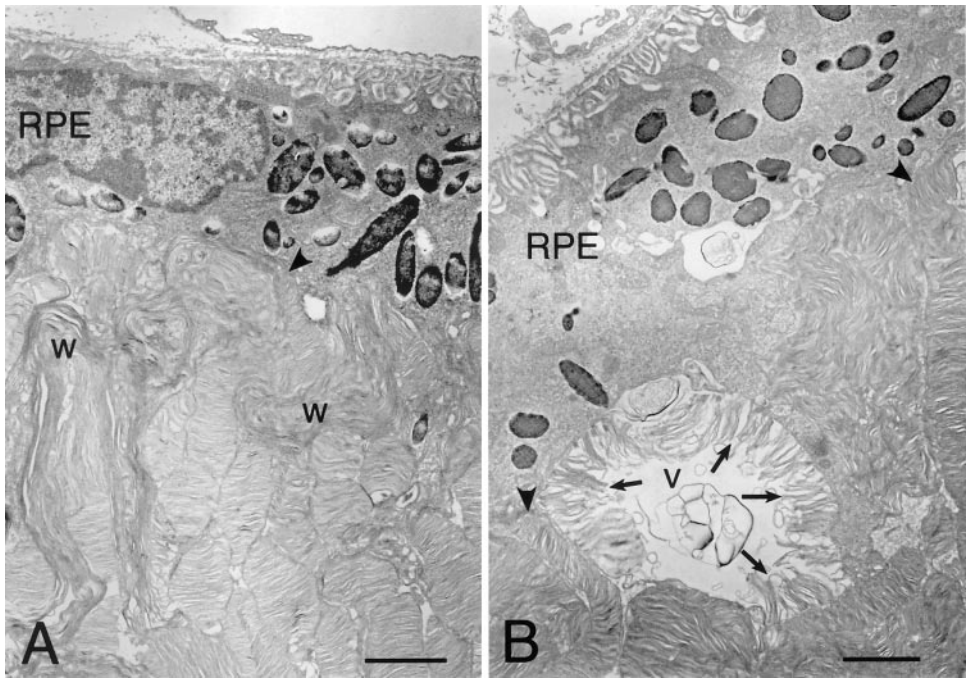

FIGURE 6. Electron micrographs of *mer*^{kd} mouse retinas. (**A**) At P21, some OS reach nearly to the RPE cell surface (*arrowhead*) and are relatively intact, although less organized than OS in age-matched WT mice. Large rounded and elongated whorls (w) of membranes are formed by disorganized OS and RPE processes. (**B**) At P37, the OS zone is mostly a debris zone, although some fragments of OS are still present, and some reach the RPE cell surface (*arrowheads*). A large vacuolated profile (v) is shown with fragments of OS disc membranes (*arrows*) in its periphery. Bar, 2 μm.

copy, the vacuoles almost always appeared to contain fragments of OS membranes (Fig. 6B), which were observed even when the vacuoles were present in or near the degenerating inner segment zone.

Invading Cells

A few invading macrophages or microglia[59,60] in each retinal section were found in the ONL as early as P15, although in the absence of specific stains, these were difficult to distinguish from developing cone nuclei. By P20, a few invading cell nuclei could clearly be seen in the ONL, and occasionally in the OS zone. By P25, distinctly more cells were found in both layers, and the number peaked at P33 to P45 (e.g., Figs. 2C, 4B), where 25 to 60 invading cells per section could be seen in each layer. During this peak period and through approximately P60, cytoplasmic inclusions and lipid droplets occasionally were seen in the invading cells (Figs. 2C, 4B), but almost none of the cells appeared engorged with ingested material, similar to the appearance at these stages of degeneration in RCS rats.[61,62]

Late-Stage Changes

At late stages of degeneration after most PRs and the OS debris zone have been lost, a number of features seen in RCS rats[61] were observed in *mer*^{kd} mice. The RPE showed small focal regions of thinning as early as P45, with several such regions in both hemispheres at P77 and older (Fig. 10A), yet some regions of RPE appeared thicker than normal. Retinal capillaries invaded the RPE beginning at approximately 6 months of age (Figs. 10B, 10C), and pigmented RPE cells invaded the retina and localized along retinal blood vessels beginning at approximately 8 months of age (Figs. 10B–D). Some of the pigmented cells or their processes were found to cuff small capillaries (Fig. 10C), and some migrated to the nerve fiber layer of the retina (Fig. 10C). Also, beginning at approximately 6 months of age, strands of nuclei that clearly had been displaced from the inner nuclear layer began to appear crossing the inner plexiform layer toward the ganglion cell layer (Fig. 10D). These displaced cells have been shown in RCS rats to result from vascular tortuosity.[63]

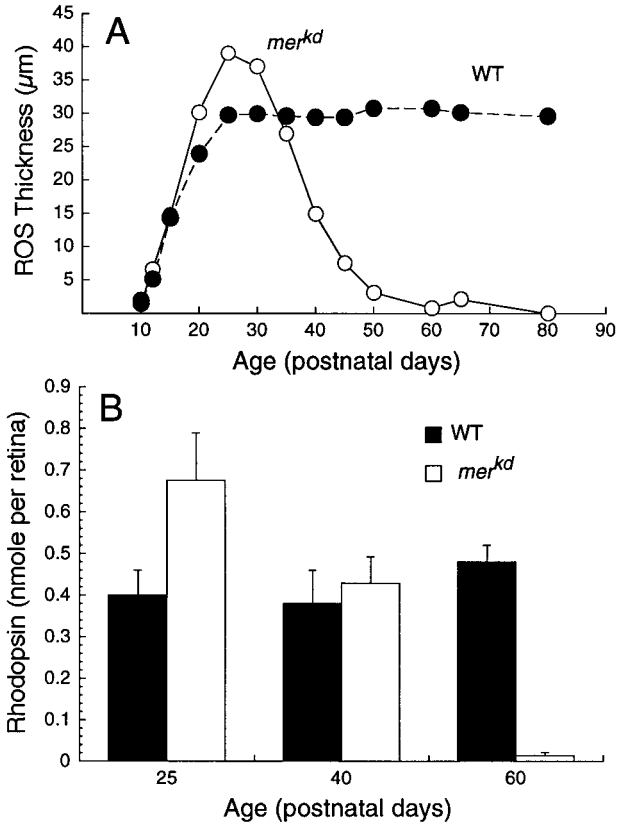

FIGURE 7. Rod OS grow abnormally long, and whole eye rhodopsin concentration is increased early in the degeneration in *mer*^{kd} mice. (**A**) Rod OS lengths are greater in *mer*^{kd} than in WT mice at young ages. Each point represents the mean of two to seven eyes measured (Table 1). (**B**) At P25, whole-eye rhodopsin concentration is increased by 67% compared with WT ($P < 0.005$). Bars represent the mean ± SEM of results in 8 to 20 eyes (Table 1).

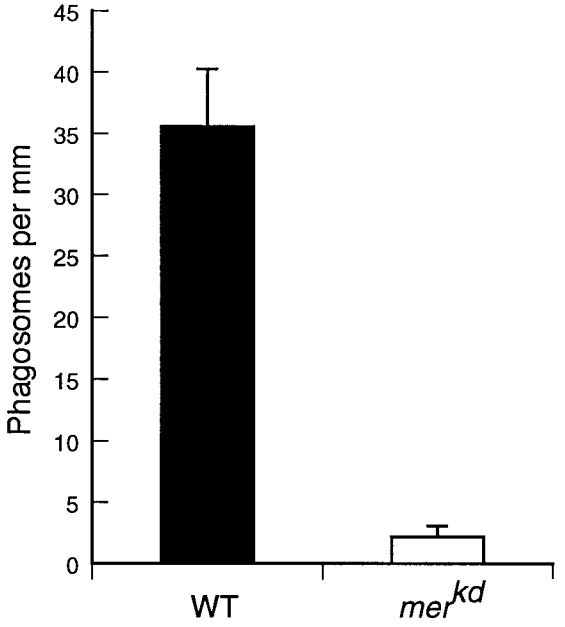

FIGURE 8. Counts of phagosomes in RPE cell processes and cell bodies during the peak of rod OS disc shedding at 1 to 1.5 hours after the onset of light. The WT mice show a typical burst of shedding, whereas very few possible phagosomes are present in *mer*^{kd} mice ($P < 0.0005$). (See text for a discussion of the ambiguities of identification of phagosomes in *mer*^{kd} mice.) For each genotype, the mean ± SD is based on pooled results in four mice, two at P15 and two P20, with all phagosomes counted in an entire retinal section from each animal (>4 mm in length).

Correlations between Retinal Structure and Function

A rapid and progressive loss of retinal function with age was apparent in *mer*^{kd} mice (Fig. 11). Representative examples of scotopic and photopic ERG recordings from a WT mouse at P30 and from *mer*^{kd} mice of different ages are shown in Figures 11A and 11B, respectively. At the youngest age examined (P20), *mer*^{kd} scotopic a- and b-wave amplitudes were significantly lower than normal ($P \leq 0.001$ and $P \leq 0.0005$, respectively; Figs. 11A, 11D, 12A). In contrast, photopic b-wave amplitudes were not significantly different from normal until *mer*^{kd} mice reached P33 (Figs. 11B, 11D, 12A, 12B). At this age and beyond, photopic amplitudes were significantly lower than normal ($P \leq 0.04$; Figs. 11B, 12B–D). Compared with WT, scotopic and photopic implicit times after P33 were delayed by approximately 75% ($P < 0.0001$) and 30% ($P < 0.02$), respectively. Interpretation of the scotopic a-wave implicit time was complicated at advanced stages of degeneration (P36 and beyond), because of interference from the cornea-negative STR (Fig. 11A). Both scotopic a- and b-wave and photopic b-wave amplitudes declined rapidly, and implicit times increased with age. No clear ERG a- or b-waves were detectable beyond P40 in most mice (Figs. 11A, 11B, 11D, 12D), although small-amplitude scotopic and photopic b-waves were seen in a few mice at ages P58 to P65 (Fig. 12).

As in most retinal degenerations,[20,64–68] scotopic ERG amplitudes decreased with age and PR loss in *mer*^{kd} mice. The ONL thickness decreased with scotopic a-wave ($r^2 = 0.83$, $P < 0.0001$) and b-wave ($r^2 = 0.82$, $P < 0.0001$) and photopic b-wave ($r^2 = 0.75$, $P < 0.0001$) amplitudes (Fig. 11D). However, as seen in Figure 11D, the positive correlation between ERG amplitudes and ONL thickness in *mer*^{kd} mice was not as strong as that which has been observed in other retinal degenerations[65]; ERG amplitudes declined significantly earlier than ONL thickness. We considered that the persistence of pyknotic nuclei may have resulted in artificially thick ONL measurements. In an effort to correct for this possibility, we subtracted from the ONL thickness (Fig. 11D) the percentage of pyknotic nuclei at each age (Fig. 4A). When the estimate of ONL thickness that included only nonpyknotic cells was compared with the scotopic a- and b-wave and photopic b-wave amplitudes, a much stronger positive correlation was evident (Fig. 11D). The corrected ONL thickness, which excluded the percentage of pyknotic cells, decreased with scotopic a-wave ($r^2 = 0.96$, $P < 0.005$) and b-wave ($r^2 = 0.93$, $P < 0.01$) and photopic b-wave ($r^2 = 0.82$, $P < 0.05$) amplitudes (Fig. 11D). These correlation coefficients are comparable to those reported by others for light-damaged rats[68] and transgenic rats with rhodopsin mutations.[65] Thus, in those instances in which pyknotic nuclei persist, a correction in the ONL thickness must be made to obtain an accurate estimate of the number of viable PR cells for structural–functional correlations.

The progressive loss of retinal function in *mer*^{kd} mice was also apparent from a plot of amplitude versus intensity for scotopic and photopic responses at different ages (Fig. 12). At

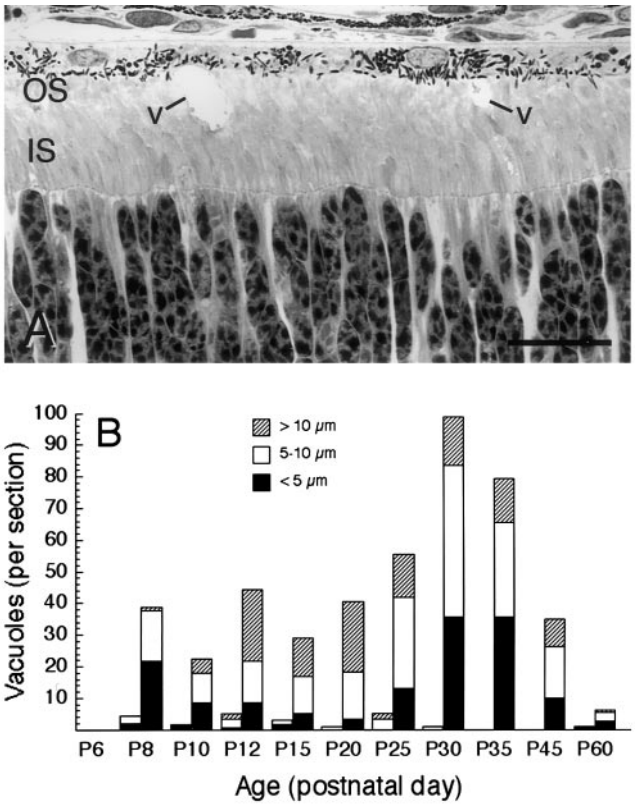

FIGURE 9. Vacuoles are present in the OS layer throughout the course of retinal degeneration in *mer*^{kd} mice. (**A**) A light micrograph at P10, when early discrete OS are visible, showing vacuoles (v) in the developing OS zone. Bar, 20 μm. (**B**) Histogram showing the number of vacuoles per retinal section seen at several ages in WT and *mer*^{kd} mice. At each age, the *left* bar in each pair is WT, and the *right* bar is *mer*^{kd}. One retinal section per mouse was examined, and each bar represents the mean of results in two to three mice. Vacuoles were tabulated across the entire retinal section, except for approximately 130 μm from each side of the optic nerve head and approximately 275 μm from each ora serrata. Only vacuoles that were ovoid or spherical in shape were tabulated. Thin vertically oriented profiles that appeared to be artifactual spaces between OS (e.g., Fig. 5A) were not included. Vacuoles were tabulated by size, as indicated in the legend. Neither WT nor *mer*^{kd} mice at P2, P4, or P6 show vacuoles (P2 and P4 not illustrated), and no vacuoles are found in WT retinas at P35 or P45.

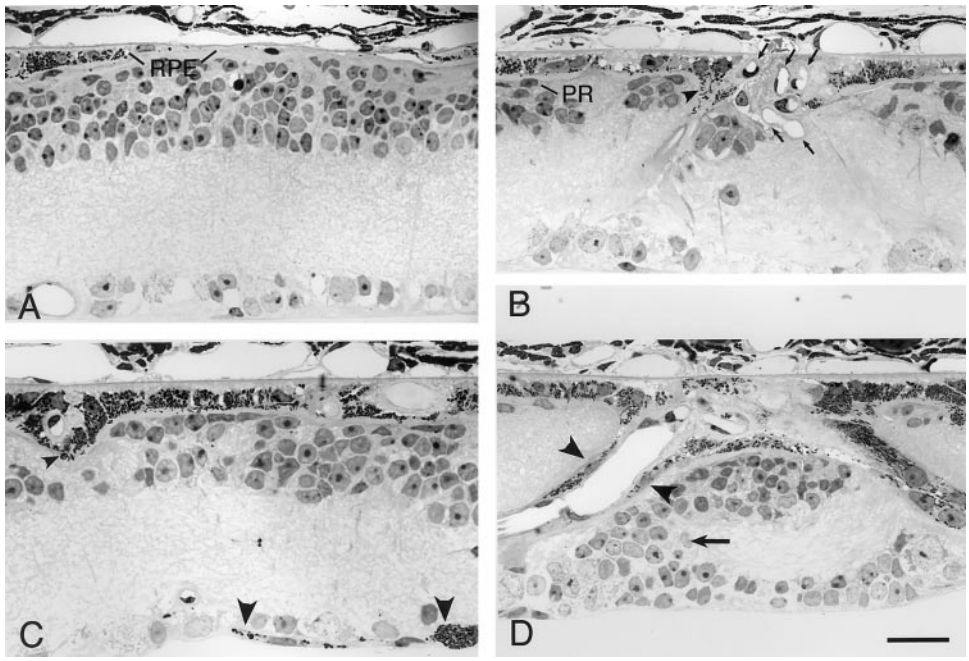

FIGURE 10. Light micrographs of mer^{kd} retinas at advanced age (P240). (**A**) The RPE cell layer is attenuated. (**B**) Retinal capillaries have invaded the RPE layer (*arrows*), and a pigmented RPE cell (*arrowhead*) appears to be migrating along a blood vessel. A single surviving cone PR nucleus is observed (PR). (**C**) A pigmented RPE cell (*small arrowhead*) surrounds a retinal capillary, and in some areas is observed in the inner retinal nerve fiber layer (*large arrowheads*). (**D**) RPE cells are associated with a retinal vessel (*arrowheads*), and cells of the inner nuclear layer have been displaced into the IPL (*arrow*). Bar, 25 μm.

the youngest age tested, P20, the maximum scotopic b-wave amplitudes were significantly lower than WT, whereas photopic amplitudes were normal (Fig. 12A). As PRs were lost with time, both scotopic and photopic amplitudes were significantly lower than WT at P33 (Fig. 12B) and P36 (Fig. 12C). At these ages, the uncorrected ONL thickness was reduced 35% ($P < 0.01$) and 60% ($P < 0.0001$) below WT, respectively. By P40, neither scotopic nor photopic b-waves were measurable in most mice (Fig. 12D).

Others have found that in RCS and light-damaged rats the scotopic b-wave threshold is more closely related to PR degeneration (i.e., the number of surviving PR nuclei) than is the maximum b-wave amplitude.[52,68] We investigated the relationship between the threshold intensity to elicit scotopic and photopic b-waves and PR degeneration in mer^{kd} mice. At the youngest ages examined, scotopic b-wave thresholds were significantly higher than normal ($P \leq 0.001$), and b-wave thresholds increased with age in mer^{kd} mice, until no b-wave was elicited at the highest stimulus intensities after P65 (Figs. 11D, 13A). In contrast, photopic thresholds were normal in mer^{kd} mice until P36, then increased rapidly with age (Fig. 13B).

Photopic responses, both amplitudes and thresholds, were better preserved than scotopic responses in mer^{kd} mice. Consistent with this, histologic analysis showed a preferential preservation of cones (Fig. 3B). In addition, mice heterozygous for the mer^{kd} mutation had normal retinal structure and function at a wide range of ages (data not shown), as is also seen in rats heterozygous for *rdy*.[69]

Scotopic Threshold Response

The STR, a cornea-negative waveform elicited at flash intensities below the b-wave threshold, has been observed in a number of animals,[70] including RCS rats[52] and WT mice.[71] We elicited the STR at low flash intensities in WT mice at all ages tested (data not shown). In young mer^{kd} mice, cornea-negative waveforms were elicited by low flash intensities similar to those observed in WT mice (Fig. 11C, arrows; Fig. 13C). This response was markedly attenuated after intravitreous injection with NMA in both WT and mer^{kd} mice (data not shown), consistent with the STR response observed in RCS rats.[52] At the youngest ages examined, the threshold to elicit the STR was not significantly different between mer^{kd} and WT mice, but at P33 and older, the STR threshold was significantly higher in mer^{kd} mice than in age-matched WT mice ($P < 0.005$; Fig. 13C). The STR threshold increased with age in mer^{kd} mice ($r^2 = 0.80$, $P < 0.0001$; Fig. 13C).

Usually after P40, and always after P65, neither scotopic nor photopic b-waves were recordable in response to the brightest stimulus intensity (+2.4 log cd sec/m^2) in mer^{kd} mice. However, the STR could be elicited even at advanced stages of PR degeneration in some mer^{kd} mice (Fig. 13D) up to P253. Thus, the STR was measurable at bright stimulus intensities when only scattered PR nuclei remained.

DISCUSSION

The retinal phenotype of mer^{kd} mice displays a striking similarity to the well-described retinal dystrophy phenotype of RCS rats. As is the case with *rdy* in RCS rats,[69] the mer^{kd} retinal phenotype is completely recessive, because mice heterozygous for the mutation have normal retinal structure and function.

Phagocytosis Defect in the RPE and PR Cell Death

The hallmark of the retinal dystrophy phenotype in RCS rats is the failure of rod OS phagocytosis by the RPE.[18,19,44] In vitro assays indicate a small but quantifiable amount of phagocytosis by the RPE of RCS rats.[72–74] An even lower level of phagocytosis has been reported in RCS rats in vivo,[73,75] but most of the illustrated inclusions in the RPE in these studies did not meet the criteria of phagosomes as they were originally defined,[45,58] and some appeared to be whorls of membranes shown previously to be formed within the RPE layer by the RPE cells.[44] Thus, it is unclear whether the defect in RCS rats results in total absence or gross reduction of OS phagocytosis by the RPE in vivo.

Our findings in the rod OS disc shedding experiments at the peak of rod OS shedding with the mer^{kd} mice were virtually identical with those in RCS rats—a gross reduction in the level of rod OS disc shedding and phagocytosis by the RPE cells, with the same degree of uncertainty in the identification of the

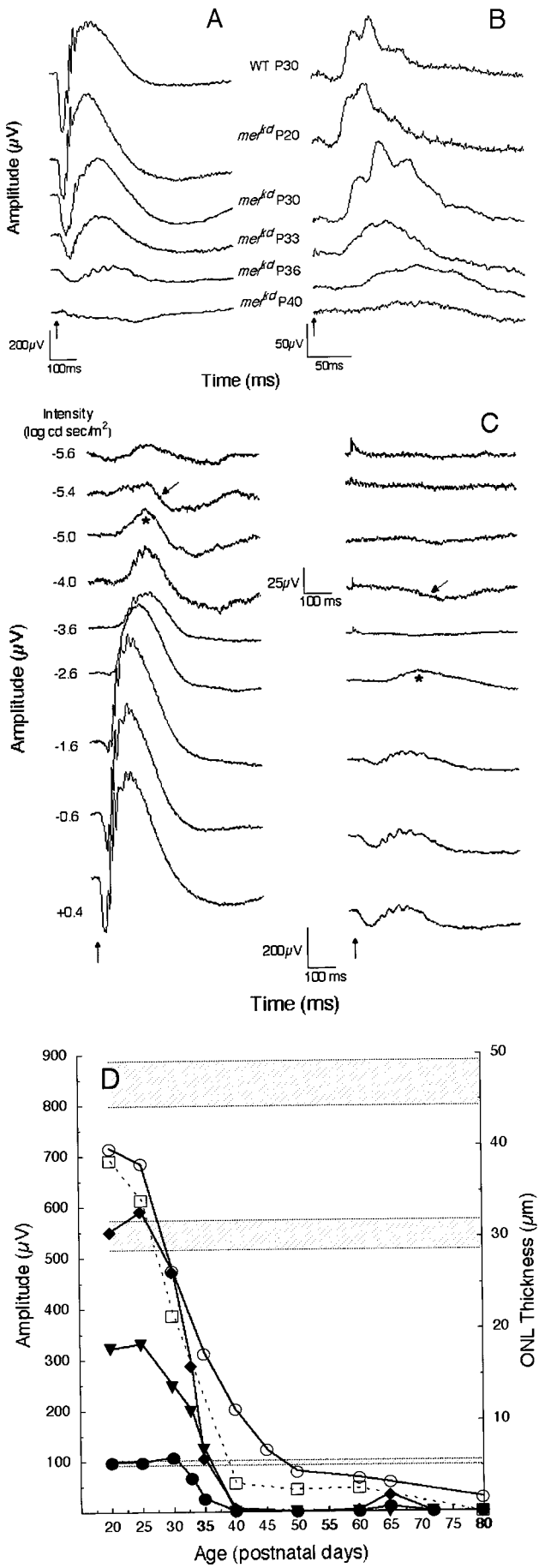

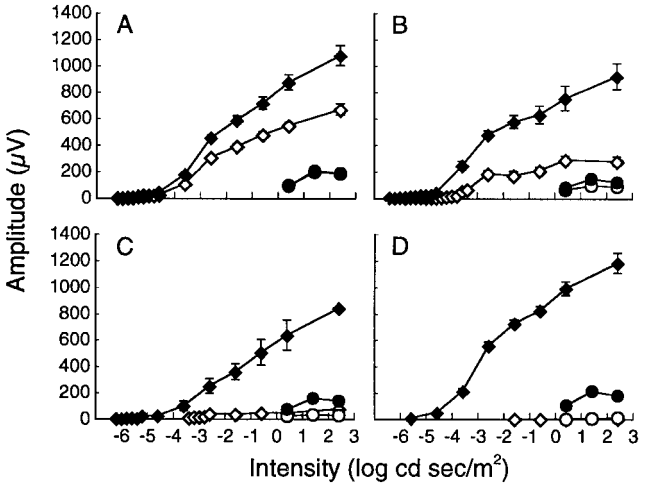

FIGURE 12. Amplitude versus stimulus intensity curves for scotopic (*diamonds*) and photopic (*circles*) b-waves in WT (*filled symbols*) and *mer*^{kd} (*open symbols*) mice at different ages. (**A**) At P20, the maximum scotopic b-wave amplitude is significantly lower than WT, whereas photopic amplitudes are normal. At P33 (**B**) and P36 (**C**) both scotopic and photopic amplitudes are lower than WT. (**D**) By P40 neither scotopic nor photopic responses are measurable in most *mer*^{kd} mice. Mean ± SEM amplitudes are shown.

very few possible phagosomes seen. Thus, in both RCS rats and *mer*^{kd} mice, it remains to be determined whether any residual normal phagocytosis of rod OS membranes by the RPE occurs in vivo. Despite this ambiguity, it is clear from the absence or near absence of phagosomes in the RPE of *mer*^{kd} mice and RCS rats that the tyrosine kinase Mer plays a major role in rod OS ingestion by the RPE in vivo.

A cascade of cytopathologic events occurs in RCS rats that ultimately leads to PR cell death. This sequence of events has been assumed to result from defective phagocytosis by the RPE. First, membranous whorls form in the OS layer adjacent to the RPE surface[19,44]; second, OS disc synthesis continues,[19,44] transiently producing longer than normal OS[19,20,44] and increased rhodopsin content in the eye[20,21,76]; third, the OS degenerate into a membranous debris zone; and fourth, PRs degenerate (for as yet unknown reasons), with preferential

FIGURE 11. Time course of ERG amplitude changes in *mer*^{kd} mice. (**A**) Representative scotopic and (**B**) photopic ERG recordings from a WT mouse at P30 (*top waveform*) and from *mer*^{kd} mice at different ages are shown. Recordings were made in response to a standard flash of 0.4 log cd sec/m^2. Scotopic a- and b-wave amplitudes are lower than normal at the earliest age tested (P20) and rapidly decline with age. Photopic amplitudes are normal until P30 before rapidly declining with age. (**C**) Representative scotopic ERG waveforms from WT (*left*) and *mer*^{kd} (*right*) mice at P36. The STR (*large arrows*) and b-wave (★) thresholds are elevated 1.5 and 2.5 log units, respectively, and b- and a-wave amplitudes are reduced in the *mer*^{kd} mouse. *Arrows*: stimulus onset. (**D**) *Horizontal hatched zones*: delineation of WT mean ± SEM amplitudes for scotopic b-waves (*top zone*), scotopic a-waves (*middle zone*), and photopic b-waves (*bottom zone*). Scotopic b-wave and photopic amplitudes are measured in response to a standard flash of 0.4 log cd sec/m^2. Scotopic a-waves are in response to a bright flash of 2.4 log cd sec/m^2. Mean amplitudes for (♦) scotopic b-waves, (▼) scotopic a-waves, and (●) photopic b-waves for *mer*^{kd} mice. Whereas scotopic amplitudes are lower than WT at the youngest ages tested, photopic responses remain normal until P30 before rapidly declining. The ONL thickness (○) decline in *mer*^{kd} mice at a rate slower than the rate of loss of ERG amplitude. The modified ONL thickness (□) reflects only nonpyknotic nuclei, which decline at a rate comparable to the rates of loss of ERG amplitude.

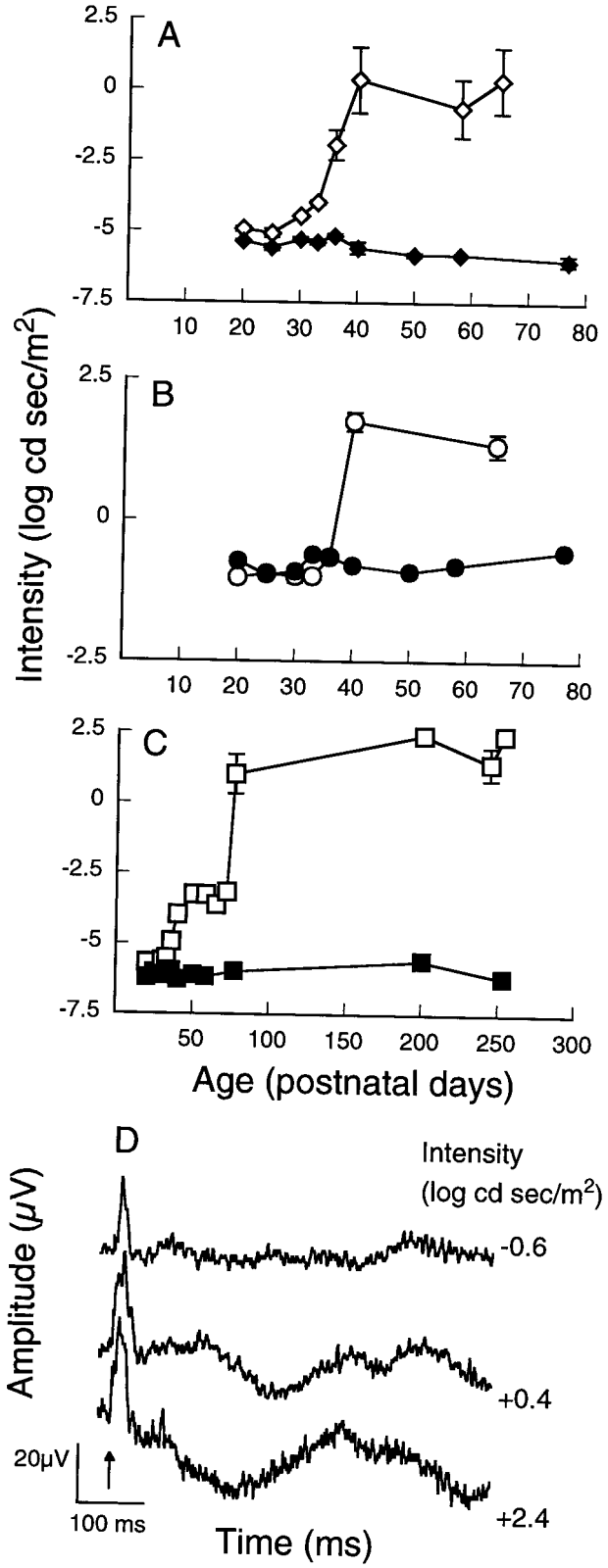

FIGURE 13. Time course of ERG threshold changes in WT and *mer*^{kd} mice. (**A**) Scotopic b-wave thresholds in *mer*^{kd} (◇) are elevated above those in WT (◆) at the earliest ages tested. (**B**) Photopic thresholds in *mer*^{kd} (○) are not different from those in WT (●) until P40. (**C**) STR thresholds in *mer*^{kd} (□) are not different from those in WT (■) until P33. Mean ± SEM thresholds are shown. (**D**) In some *mer*^{kd} mice, a small amplitude STR is measurable in response to the highest stimulus intensities, even after advanced PR loss at P253.

cone survival.[54] The presence in *mer*^{kd} mice of these characteristic features of RCS rats demonstrates that Mer tyrosine kinase serves the same function(s) in the retinas of these two rodents and suggests that the phagocytosis defect underlies these features of the retinal dystrophy phenotype.

Differences in the *mer*^{kd} Mouse and RCS Rat Retinal Phenotypes

Certain temporal aspects of the retinal degenerations differ between the two types of rodent models. Pigmented RCS rat retinas degenerate at a slower rate than those of pink-eyed (nonpigmented) RCS rats.[21] The onset and rate of degeneration in the *mer*^{kd} mice, which are pigmented, are similar to and even slightly more rapid than those of pink-eyed RCS rats (Fig. 3A). The temporal relationship between PR cell loss, debris membrane loss, and rhodopsin loss also differs between *mer*^{kd} mice and RCS rats. In pink-eyed RCS rats, some OS debris persists for 2 to 3 weeks after the loss of most PR cell nuclei. When the pink-eyed RCS rats are dark-reared or when pigmented rats are raised in cyclic light, an even greater amount of debris remains for several months after the loss of most PR nuclei.[21] As noted, pigmented *mer*^{kd} mice showed a rate of PR loss similar to that of pink-eyed RCS rats. However, the OS debris was lost concomitantly with the PR nuclei and did not persist for any substantive period, at least in *mer*^{kd} mice reared in cyclic light.

The reasons for the temporal differences between the mice and rats are unclear, and in fact, given the similarity of the other phenotypic characteristics, a significant persistence of the OS debris would have been expected in *mer*^{kd} mice because of their eye pigmentation. Some possible explanations include (1) species differences between rats and mice such as more rapid development and degeneration in mice, (2) differences in retinal irradiance due to eye size or to the influence of eye pigmentation,[77] (3) differences in background genes that may regulate the degenerative response to light,[78] (4) differences in stability of rhodopsin in the degenerating membranes, (5) differences in the ability of invading phagocytes to remove the OS debris, or (6) a combination of these factors.

Persistent Pyknotic Nuclei

A remarkable feature of *mer*^{kd} mice is the persistence of pyknotic nuclei at most stages of retinal degeneration, with some coalescing and forming large masses of heterochromatin in the ONL. This unusual phenomenon is also seen in RCS rats,[21] but not in other hereditary retinal degenerations, including *rd/rd*,[79] *nr/nr*,[80] *pcd/pcd*,[81] *rds/rds*,[82] or transgenic rats with rhodopsin mutations (Fig. 4A), or in light-induced degenerations.[43,83,84] Thus, the persistence of pyknotic PR nuclei appears to be unique to retinal degenerations caused by mutations in Mer tyrosine kinase. In all PR degenerations examined to date, including that in RCS rats,[62] PR cell death occurs through the process of apoptosis.[85–87] It is generally accepted that the half-life of apoptotic nuclei is relatively short, and therefore it is surprising that pyknotic nuclei persist in rodents with mutations in Mer tyrosine kinase.

It is likely that delayed clearance of pyknotic PR cells from the ONL is a direct consequence of a generalized defect in phagocytosis of postnatal apoptotic cells in *mer*^{kd} mice. The *mer*^{kd} mutation has already been shown to cause abnormal clearance by macrophages of dying thymocytes and lymphocytes.[41] Pyknotic PR cells are most likely cleared by migrating phagocytes, either blood-derived monocytes[59,61] or activated microglia,[60] and *Mer* is known to be expressed in the monocyte/macrophage lineage, as well as a number of other cell types throughout the body.[88,89] Defective clearance of apoptotic cells in *mer*^{kd} mice results in increased reactivity to self

antigens.[41] Humans with retinal degenerations due to *MERTK* mutations[38] may have as yet unrecognized systemic defects in the clearance of apoptotic cells, which could predispose toward autoimmune disease.

Earliest Phenotypic Expression of the Mer Mutation

Large vacuoles in the OS zone were seen at most ages during the course of retinal degeneration in mer^{kd} mice. This feature also has been observed in RCS rats (LaVail MM, unpublished observations, 2000) and is evident in several well-fixed histologic preparations of RCS retinas.[19–21] Such vacuoles are not regularly observed in several other retinal degenerations, including *pcd/pcd*, *nr/nr*, *rd/rd*, or *rds/rds* mutant mice or in transgenic rodents with rhodopsin mutations (LaVail MM, unpublished observations, 2001). The vacuoles in mer^{kd} mice and RCS rats appear similar to "exploded" OS—fixation artifacts that result from abnormal osmotic conditions—but the vacuoles were observed in well-fixed mer^{kd} tissues and very few were seen in WT tissues. Similar OS vacuoles have been demonstrated in mice that have no interphotoreceptor retinoid-binding protein (IRBP) at as early as 11 days of age[90] and as late as 6 months of age.[91] However, the vacuolated rod OS found at very early ages in RCS rats (and presumably mer^{kd} mice) are apparently not due to a deficit in IRBP, because abnormalities in concentration or distribution of IRBP do not appear in RCS rats until P15 to P18, or later.[92,93]

These facts suggest that complete loss of *Mer* function may lead to an abnormal osmotic environment around OS and that the vacuoles may result from interphotoreceptor matrix abnormalities, either in osmotic composition or in abnormal transport and recycling of fatty acids.[90,91] The vacuoles were present at the earliest time when discrete OS were observed (P8) and, as such, they represent the earliest histologic abnormality that has been reported in animals with *Mer* mutations, occurring before other OS abnormalities and significantly before PR cell death. It remains to be determined precisely how Mer defects lead to vacuoles in the outer retina and what role, if any, the vacuoles play in PR cell death.

Conclusion

The mer^{kd} mouse strain displays a retinal degeneration phenotype almost identical with that of the RCS rat. This mouse model may be particularly useful for studying the role of Mer in PR-RPE cell interactions, phagocytosis, and retinal degeneration, given the powerful tools available for forward and reverse genetic studies in mice.

Acknowledgments

The authors thank Jose Velarde, Nancy Lawson, and Dean Cruz for technical assistance and Dean Bok for advice in performing the rhodopsin analysis.

References

1. The United States Census Bureau. Population Projections of the United States by Age, Sex, Race, and Hispanic Origin: 1995 to 2050. In: *Current Population Reports, Series P25-1130.* Washington DC: U.S. Census Bureau; 1995.
2. Young RW. Pathophysiology of age-related macular degeneration. *Surv Ophthalmol.* 1987;31:291–306.
3. Green WR, Harlan JBJ. Histopathologic features. In: Berger JW, Fine SL, Maguire MG, eds. *Age-Related Macular Degeneration.* St. Louis: Mosby, Inc.; 1999:81–154.
4. Zarbin MA. Age-related macular degeneration: review of pathogenesis. *Eur J Ophthalmol.* 1998;8:199–206.
5. Petrukhin K, Koisti MJ, Bakall B, et al. Identification of the gene responsible for Best macular dystrophy. *Nat Genet.* 1998;19:241–247.
6. Marmorstein AD, Marmorstein LY, Rayborn M, Wang X, Hollyfield JG, Petrukhin K. Bestrophin, the product of the Best vitelliform macular dystrophy gene (VMD2), localizes to the basolateral plasma membrane of the retinal pigment epithelium. *Proc Natl Acad Sci USA.* 2000;97:12758–12763.
7. Weng J, Mata NL, Azarian SM, Tzekov RT, Birch DG, Travis GH. Insights into the function of Rim protein in photoreceptors and etiology of Stargardt's disease from the phenotype in *abcr* knockout mice. *Cell.* 1999;98:13–23.
8. Steinmetz RL, Polkinghorne PC, Fitzke FW, Kemp CM, Bird AC. Abnormal dark adaptation and rhodopsin kinetics in Sorsby's fundus dystrophy. *Invest Ophthalmol Vis Sci.* 1992;33:1633–1636.
9. Jacobson SG, Cideciyan AV, Regunath G, et al. Night blindness in Sorsby's fundus dystrophy reversed by vitamin A. *Nat Genet.* 1995;11:27–32.
10. Gu SM, Thompson DA, Srikumari CR, et al. Mutations in *RPE65* cause autosomal recessive childhood-onset severe retinal dystrophy. *Nat Genet.* 1997;17:194–197.
11. Marlhens F, Bareil C, Griffoin JM, et al. Mutations in *RPE65* cause Leber's congenital amaurosis. *Nat Genet.* 1997;17:139–141.
12. Morimura H, Fishman GA, Grover SA, Fulton AB, Berson EL, Dryja TP. Mutations in the RPE65 gene in patients with autosomal recessive retinitis pigmentosa or Leber congenital amaurosis. *Proc Natl Acad Sci USA.* 1998;95:3088–3093.
13. Thompson DA, Gyurus P, Fleischer LL, et al. Genetics and phenotypes of *RPE65* mutations in inherited retinal degeneration. *Invest Ophthalmol Vis Sci.* 2000;41:4293–4299.
14. Lotery AJ, Namperumalsamy P, Jacobson SG, et al. Mutation analysis of 3 genes in patients with Leber congenital amaurosis. *Arch Ophthalmol.* 2000;118:538–543.
15. Strauss O, Stumpff F, Mergler S, Wienrich M, Wiederholt M. The Royal College of Surgeons rat: an animal model for inherited retinal degeneration with a still unknown genetic defect. *Acta Anat.* 1998;162:101–111.
16. LaVail MM. Legacy of the RCS rat: impact of a seminal study on retinal cell biology and retinal degenerative diseases. In: Kolb H, Ripps H, Wu S, eds. *Progress in Brain Research.* Paris: Elsevier Science; 2001:617–627.
17. Mullen RJ, LaVail MM. Inherited retinal dystrophy: primary defect in pigment epithelium determined with experimental rat chimeras. *Science.* 1976;192:799–801.
18. Herron WL, Riegel BW, Myers OE, Rubin ML. Retinal dystrophy in the rat: a pigment epithelial disease. *Invest Ophthalmol.* 1969;8:595–604.
19. Bok D, Hall MO. The role of the pigment epithelium in the etiology of inherited retinal dystrophy in the rat. *J Cell Biol.* 1971;49:664–682.
20. Dowling JE, Sidman RL. Inherited retinal dystrophy in the rat. *J Cell Biol.* 1962;14:73–109.
21. LaVail MM, Battelle BA. Influence of eye pigmentation and light deprivation on inherited retinal dystrophy in the rat. *Exp Eye Res.* 1975;21:167–192.
22. D'Cruz PM, Yasumura D, Weir J, et al. Mutation of the receptor tyrosine kinase gene *Mertk* in the retinal dystrophic RCS rat. *Hum Mol Genet.* 2000;9:645–651.
23. Nagata K, Ohashi K, Nakano T, et al. Identification of the product of growth arrest-specific gene 6 as a common ligand for Axl, Sky, and Mer receptor tyrosine kinases. *J Biol Chem.* 1996;271:30022–30027.
24. Chen J, Carey K, Godowski PJ. Identification of Gas6 as a ligand for Mer, a neural cell adhesion molecule related receptor tyrosine kinase implicated in cellular transformation. *Oncogene.* 1997;14:2033–2039.
25. Varnum BC, Young C, Elliott G, et al. Axl receptor tyrosine kinase stimulated by the vitamin K-dependent protein encoded by growth-arrest-specific gene 6. *Nature.* 1995;373:623–626.
26. Mark MR, Chen J, Hammonds RG, Sadick M, Godowsk PJ. Characterization of Gas6, a member of the superfamily of G domain-containing proteins, as a ligand for Rse and Axl. *J Biol Chem.* 1996;271:9785–9789.

27. Nakano T, Ishimoto Y, Kishino J, et al. Cell adhesion to phosphatidylserine mediated by a product of growth arrest-specific gene 6. *J Biol Chem.* 1997;272:29411–29414.
28. Fadok VA, Bratton DL, Frasch SC, Warner ML, Henson PM. The role of phosphatidylserine in recognition of apoptotic cells by phagocytes. *Cell Death Diff.* 1998;5:551–562.
29. Hall MO, Prieto AL, Obin MS, et al. Outer segment phagocytosis by cultured retinal pigment epithelial cells requires gas6. *Exp Eye Res.* 2001;73:509–520.
30. Feng W, Yasumura D, Matthes MT, LaVail MM, Vollrath D. Mertk triggers uptake of photoreceptor outer segments during phagocytosis by cultured retinal pigment epithelial cells. *J Biol Chem.* 2002;277:17016–17022.
31. McLaughlin BJ, Cooper NG, Shepherd VL. How good is the evidence to suggest that phagocytosis of ROS by RPE is receptor mediated? In: Osborne N, Chader G, eds. *Progress in Retinal and Eye Research.* Oxford, UK: Pergamon Press; 1994:147–164.
32. Hall MO, Burgess BL, Abrams TA, Ershov AV, Gregory CY. Further studies on the identification of the phagocytosis receptor of rat retinal pigment epithelial cells. *Exp Eye Res.* 1996;63:255–264.
33. Finnemann SC, Bonilha VL, Marmorstein AD, Rodriguez-Boulan E. Phagocytosis of rod outer segments by retinal pigment epithelial cells requires alpha(v)beta5 integrin for binding but not for internalization. *Proc Natl Acad Sci USA.* 1997;94:12932–12937.
34. Ryeom SW, Sparrow JR, Silverstein RL. CD36 participates in the phagocytosis of rod outer segments by retinal pigment epithelium. *J Cell Sci.* 1996;109:387–395.
35. Boyle D, Tien LF, Cooper NG, Shepherd V, McLaughlin BJ. A mannose receptor is involved in retinal phagocytosis. *Invest Ophthalmol Vis Sci.* 1991;32:1464–1470.
36. Shepherd VL, Tarnowski BI, McLaughlin BJ. Isolation and characterization of a mannose receptor from human pigment epithelium. *Invest Ophthalmol Vis Sci.* 1991;32:1779–1784.
37. Vollrath D, Feng W, Duncan JL, et al. Correction of the retinal dystrophy phenotype of the RCS rat by viral gene transfer of *Mertk. Proc Natl Acad Sci USA.* 2001;98:12584–12589.
38. Gal A, Li Y, Thompson DA, et al. Mutations in MERTK, the human orthologue of the RCS rat retinal dystrophy gene, cause retinitis pigmentosa. *Nat Genet.* 2000;26:270–271.
39. Lu Q, Gore M, Zhang Q, et al. Tyro-3 family receptors are essential regulators of mammalian spermatogenesis. *Nature.* 1999;398:723–728.
40. Camenisch TD, Koller BH, Earp HS, Matsushima GK. A novel receptor tyrosine kinase, Mer, inhibits TNF-α production and lipopolysaccharide-induced endotoxic shock. *J Immunol.* 1999; 162:3498–3503.
41. Scott RS, McMahon EJ, Pop SM, et al. Phagocytosis and clearance of apoptotic cells is mediated by MER. *Nature.* 2001;411:207–211.
42. Michon JJ, Li ZL, Shioura N, Anderson RJ, Tso MO. A comparative study of methods of photoreceptor morphometry. *Invest Ophthalmol Vis Sci.* 1991;32:280–284.
43. LaVail MM, Gorrin GM, Repaci MA, Thomas LA, Ginsberg HM. Genetic regulation of light damage to photoreceptors. *Invest Ophthalmol Vis Sci.* 1987;28:1043–1048.
44. LaVail MM, Sidman RL, O'Neil D. Photoreceptor-pigment epithelial cell relationships in rats with inherited retinal degeneration: radioautographic and electron microscope evidence for a dual source of extra lamellar material. *J Cell Biol.* 1972;53:185–209.
45. LaVail MM. Rod outer segment disk shedding in rat retina: relationship to cyclic lighting. *Science.* 1976;194:1071–1074.
46. Knudsen P, Hubbell WL. Stability of rhodopsin in detergent solutions. *Membr Biochem.* 1978;1:297–322.
47. De Grip WJ. Thermal stability of rhodopsin and opsin in some novel detergents. *Methods Enzymol.* 1982;81:256–265.
48. Wald G, Brown PK. The molar extinction of rhodopsin. *J Gen Physiol.* 1953;37:189–200.
49. Peachey NS, Goto Y, al-Ubaidi MR, Naash MI. Properties of the mouse cone-mediated electroretinogram during light adaptation. *Neurosci Lett.* 1993;162:9–11.
50. Vaegan, Millar TJ. Effect of kainic acid and NMDA on the pattern electroretinogram, the scotopic threshold response, the oscillatory potentials and the electroretinogram in the urethane anaesthetized cat. *Vision Res.* 1994;34:1111–1125.
51. Robson JG, Frishman LJ. Response linearity and kinetics of the cat retina: the bipolar cell component of the dark-adapted electroretinogram. *Vis Neurosci.* 1995;12:837–850.
52. Bush RA, Hawks KW, Sieving PA. Preservation of inner retinal responses in the aged Royal College of Surgeons rat: evidence against glutamate excitotoxicity in photoreceptor degeneration. *Invest Ophthalmol Vis Sci.* 1995;36:2054–2062.
53. Hughes A. A schematic eye for the rat. *Vision Res.* 1979;19:569–588.
54. LaVail MM. Analysis of neurological mutants with inherited retinal degeneration. Friedenwald Lecture. *Invest Ophthalmol Vis Sci.* 1981;21:638–657.
55. Steinberg RH, Flannery JG, Naash M, et al. Transgenic rat models of inherited retinal degeneration caused by mutant opsin genes [ARVO Abstract]. *Invest Ophthalmol Vis Sci.* 1996;37(3):**S**698. Abstract nr 3190.
56. Besharse JC, Hollyfield JG. Turnover of mouse photoreceptor outer segments in constant light and darkness. *Invest Ophthalmol Vis Sci.* 1979;18:1019–1024.
57. Grace MS, Chiba A, Menaker M. Circadian control of photoreceptor outer segment membrane turnover in mice genetically incapable of melatonin synthesis. *Vis Neurosci.* 1999;16:909–918.
58. Young RW, Bok D. Participation of the retinal pigment epithelium in the rod outer segment renewal process. *J Cell Biol.* 1969;42: 392–403.
59. Essner E, Gorrin G. An electron microscopic study of macrophages in rats with inherited retinal dystrophy. *Invest Ophthalmol Vis Sci.* 1979;18:11–25.
60. Thanos S. Sick photoreceptors attract activated microglia from the ganglion cell layer: a model to study the inflammatory cascades in rats with inherited retinal dystrophy. *Brain Res.* 1992;588:21–28.
61. LaVail MM. The retinal pigment epithelium in mice and rats with inherited retinal degeneration. In: Zinn KM, Marmor MF, eds. *The Retinal Pigment Epithelium.* Cambridge, MA: Harvard University Press; 1979:357–380.
62. Tso MO, Zhang C, Abler AS, et al. Apoptosis leads to photoreceptor degeneration in inherited retinal dystrophy of RCS rats. *Invest Ophthalmol Vis Sci.* 1994;35:2693–2699.
63. Villegas-Perez MP, Lawrence JM, Vidal-Sanz M, LaVail MM, Lund RD. Ganglion cell loss in RCS rat retina: a result of compression of axons by contracting intraretinal vessels linked to the pigment epithelium. *J Comp Neurol.* 1998;392:58–77.
64. Kedzierski W, Lloyd M, Birch DG, Bok D, Travis GH. Generation and analysis of transgenic mice expressing P216L-substituted rds/peripherin in rod photoreceptors. *Invest Ophthalmol Vis Sci.* 1997;38:498–509.
65. Machida S, Kondo M, Jamison JA, et al. P23H rhodopsin transgenic rat: correlation of retinal function with histopathology. *Invest Ophthalmol Vis Sci.* 2000;41:3200–3209.
66. Nishikawa S, Cao W, Yasumura D, et al. Comparing the ERG to retinal morphology in transgenic rats with inherited degenerations caused by mutant opsin genes [ARVO Abstract]. *Invest Ophthalmol Vis Sci.* 1997;38(4):**S**33. Abstract nr 1415.
67. Toda K, Bush RA, Humphries P, Sieving PA. The electroretinogram of the rhodopsin knockout mouse. *Vis Neurosci.* 1999;16:391–398.
68. Sugawara T, Sieving PA, Bush RA. Quantitative relationship of the scotopic and photopic ERG to photoreceptor cell loss in light damaged rats. *Exp Eye Res.* 2000;70:693–705.
69. LaVail MM. Photoreceptor characteristics in congenic strains of RCS rats. *Invest Ophthalmol Vis Sci.* 1981;20:671–675.
70. Sieving PA, Frishman LJ, Steinberg RH. Scotopic threshold response of proximal retina in cat. *J Neurophysiol.* 1986;56:1049–1061.
71. Saszik SM, Robson JG, Frishman LJ. The scotopic threshold response of the dark-adapted electroretinogram of the mouse. *J Physiol.* 2002;543:899–916.
72. Edwards RB. Culture of rat retinal pigment epithelium. *In Vitro.* 1977;13:301–304.
73. Tamai M, O'Brien PJ. Retinal dystrophy in the RCS rat: in vivo and in vitro studies of phagocytic action of the pigment epithelium on the shed rod outer segments. *Exp Eye Res.* 1979;28:399–411.

74. Chaitin MH, Hall MO. Defective ingestion of rod outer segments by cultured dystrophic rat pigment epithelial cells. *Invest Ophthalmol Vis Sci.* 1983;24:812–820.
75. Goldman AI, O'Brien PJ. Phagocytosis in the retinal pigment epithelium of the RCS rat. *Science.* 1978;201:1023–1025.
76. Battelle BA, LaVail MM. Rhodopsin content and rod outer segment length in albino rat eyes: modification by dark adaptation. *Exp Eye Res.* 1978;26:487–497.
77. LaVail MM, Gorrin GM, Repaci MA, Yasumura D. Light-induced retinal degeneration in albino mice and rats: strain and species differences. In: Hollyfield JG, Anderson RE, LaVail MM, eds. *Degenerative Retinal Disorders: Clinical and Laboratory Investigations.* New York: Alan R. Liss, Inc.; 1987:439–454.
78. Danciger M, Matthes MT, Yasumura D, et al. A QTL on distal chromosome 3 that influences the severity of light- induced damage to mouse photoreceptors. *Mamm Genome.* 2000;11:422–427.
79. LaVail MM, Sidman RL. C57BL-6J mice with inherited retinal degeneration. *Arch Ophthalmol.* 1974;91:394–400.
80. LaVail MM, White MP, Gorrin GM, Yasumura D, Porrello KV, Mullen RJ. Retinal degeneration in the nervous mutant mouse. I. Light microscopic cytopathology and changes in the interphotoreceptor matrix. *J Comp Neurol.* 1993;333:168–181.
81. LaVail MM, Blanks JC, Mullen RJ. Retinal degeneration in the pcd cerebellar mutant mouse. I. Light microscopic and autoradiographic analysis. *J Comp Neur.* 1982;212:217–230.
82. Sanyal S, De Ruiter A, Hawkins RK. Development and degeneration of retina in rds mutant mice: light microscopy. *J Comp Neurol.* 1980;194:193–207.
83. LaVail MM, Matthes MT, Yasumura D, Faktorovich EG, Steinberg RH. Histological method to assess photoreceptor light damage and protection by survival factors. In: LaVail MM, Hollyfield JG, Anderson RE, eds. *Degenerative Retinal Diseases.* New York: Plenum Press; 1997:369–384.
84. Faktorovich EG, Steinberg RH, Yasumura D, Matthes MT, LaVail MM. Basic fibroblast growth factor and local injury protect photoreceptors from light damage in the rat. *J Neurosci.* 1992;12:3554–3567.
85. Li Z-Y, Milam AH. Apoptosis in retinitis pigmentosa. In: Anderson RE, LaVail MM, Hollyfield JG, eds. *Degenerative Diseases of the Retina.* New York: Plenum Press; 1995:1–8.
86. Papermaster DS, Windle J. Death at an early age: apoptosis in inherited retinal degenerations. *Invest Ophthalmol Vis Sci.* 1995; 36:977–983.
87. Wong F. Photoreceptor apoptosis in animal models: implications for retinitis pigmentosa research. *Arch Ophthalmol.* 1995;113: 1245–1247.
88. Graham DK, Dawson TL, Mullaney DL, Snodgrass HR, Earp HS. Cloning and mRNA expression analysis of a novel human protooncogene, c-mer. *Cell Growth Diff.* 1994;5:647–657.
89. Graham DK, Bowman GW, Dawson TL, Stanford WL, Earp HS, Snodgrass HR. Cloning and developmental expression analysis of the murine c-*mer* tyrosine kinase. *Oncogene.* 1995;10:2349–2359.
90. Liou GI, Fei Y, Peachey NS, et al. Early onset photoreceptor abnormalities induced by targeted disruption of the interphotoreceptor retinoid-binding protein gene. *J Neurosci.* 1998;18:4511–4520.
91. Ripps H, Peachey NS, Xu X, Nozell SE, Smith SB, Liou GI. The rhodopsin cycle is preserved in IRBP "knockout" mice despite abnormalities in retinal structure and function. *Vis Neurosci.* 2000; 17:97–105.
92. Gonzalez-Fernandez F, Landers RA, Glazebrook PA, et al. An extracellular retinol-binding glycoprotein in the eyes of mutant rats with retinal dystrophy: development, localization, and biosynthesis. *J Cell Biol.* 1984;99:2092–2098.
93. Eisenfeld AJ, Bunt-Milam AH, Saari JC. Immunocytochemical localization of interphotoreceptor retinoid-binding protein in developing normal and RCS rat retinas. *Invest Ophthalmol Vis Sci.* 1985; 26:775–778.
94. Carter-Dawson LD, LaVail MM, Sidman RL. Differential effect of the *rd* mutation on rods and cones in the mouse retina. *Invest Ophthalmol Vis Sci.* 1978;17:489–498.